In vivo evidence for a lactate gradient from astrocytes to neurons

Mächler, Philipp ; Wyss, Matthias T ; Elsayed, Maha ; Stobart, Jillian ; Gutierrez, Robin ; von Faber-Castell, Alexandra ; Kaelin, Vincens ; Zuend, Marc ; San Martín, Alejandro ; Romero-Gómez, Ignacio ; Baeza-Lehnert, Felipe ; Lengacher, Sylvain ; Schneider, Bernard L ; Aebischer, Patrick ; Magistretti, Pierre J ; Barros, L Felipe ; Weber, Bruno

Abstract: The determination of lactate dynamics in brain tissue represents a challenge, partly because in vivo data at cellular resolution are not available. Here we monitored lactate in astrocytes and neurons of the primary somatosensory cortex of mice using the genetically-encoded FRET sensor Laconic in combination with two-photon laser scanning microscopy. An intravenous lactate injection rapidly increased the Laconic signal in both astrocytes and neurons, demonstrating high lactate permeability across the tissue. The signal increase was significantly smaller in astrocytes pointing to higher basal lactate levels in these cells, confirmed by a one-point in vivo calibration protocol.Trans-acceleration of the monocarboxylate transporter with pyruvate was able to reduce intracellular lactate in astrocytes but not in neurons. Collectively, this data provides in vivo evidence for a lactate gradient from astrocytes to neurons.

DOI: https://doi.org/10.1016/j.cmet.2015.10.010

Originally published at:
Mächler, Philipp; Wyss, Matthias T; Elsayed, Maha; Stobart, Jillian; Gutierrez, Robin; von Faber-Castell, Alexandra; Kaelin, Vincens; Zuend, Marc; San Martín, Alejandro; Romero-Gómez, Ignacio; Baeza-Lehnert, Felipe; Lengacher, Sylvain; Schneider, Bernard L; Aebischer, Patrick; Magistretti, Pierre J; Barros, L Felipe; Weber, Bruno (2016). In vivo evidence for a lactate gradient from astrocytes to neurons. Cell Metabolism, 23(1):94-102.
DOI: https://doi.org/10.1016/j.cmet.2015.10.010

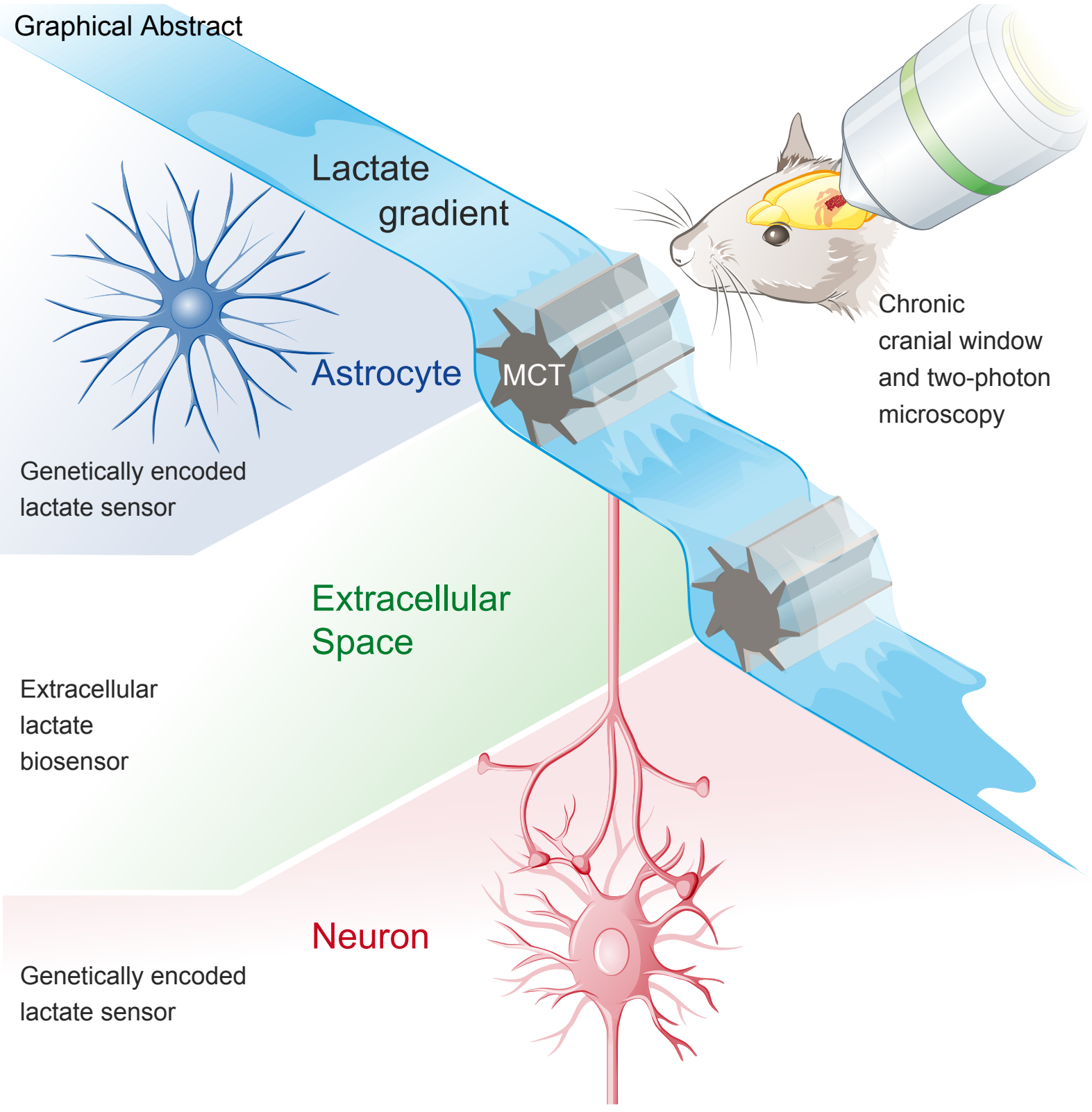
Graphical Abstract
Lactate
gradient
Astrocyte
MCT
Chronic
cranial window
and two-photon
microscopy
Genetically encoded
lactate sensor
Extracellular
Space
Extracellular
lactate
biosensor
Neuron
Genetically encoded
lactate sensor

In vivo evidence for a lactate gradient from astrocytes to neurons

Philipp Mächler[1,2,6], Matthias T. Wyss[1,2,6], Maha Elsayed[3], Jillian Stobart[1,2], Robin Gutierrez[1,4], Alexandra von Faber-Castell[1], Vincens Kaelin[1], Marc Zuend[1,2], Alejandro San Martín[4], Ignacio Romero-Gómez[4], Felipe Baeza-Lehnert[4], Sylvain Lengacher[3], Bernard L. Schneider[3], Patrick Aebischer[3], Pierre J. Magistretti[3,5], L. Felipe Barros[4] and Bruno Weber[1,2]

[1]Institute of Pharmacology and Toxicology, University of Zurich, 8057 Zurich, Switzerland

[2]Neuroscience Center Zurich, University and ETH Zurich, 8092 Zurich, Switzerland

[3]Brain Mind Institute, École Polytechnique Fédérale de Lausanne, 1015 Lausanne, Switzerland

[4]Centro de Estudios Científicos, Valdivia 5110466, Chile

[5]Division of Biological and Environmental Sciences and Engineering, KAUST, Thuwal, KSA

Correspondence: bweber@pharma.uzh.ch

[6] These authors contributed equally to this work

Running Title: *In vivo* evidence for a lactate gradient from astrocytes to neurons

Summary

The determination of lactate dynamics in brain tissue represents a challenge, partly because *in vivo* data at cellular resolution are not available. Here we monitored lactate in astrocytes and neurons of the primary somatosensory cortex of mice using the genetically-encoded FRET sensor *Laconic* in combination with two-photon laser scanning microscopy. An intravenous lactate injection rapidly increased the *Laconic* signal in both astrocytes and neurons, demonstrating high lactate permeability across the tissue. The signal increase was significantly smaller in astrocytes pointing to higher basal lactate levels in these cells, confirmed by a one-point in vivo calibration protocol.

Trans-acceleration of the monocarboxylate transporter with pyruvate was able to reduce intracellular lactate in astrocytes but not in neurons. Collectively, this data provides i*n vivo* evidence for a lactate gradient from astrocytes to neurons.

Introduction

The energy demand of mammalian brain tissue is met mainly by degradation of blood borne glucose. Classical experiments with radiolabeled substrates showed label incorporation into glutamate and glutamine in a manner suggestive of two separate tricarboxylic acid cycles, a 'large' and a 'small' compartment (Van den Berg et al., 1969), which were assigned to neurons and astrocytes respectively using immunohistochemical techniques (Martinez-Hernandez et al., 1977). The concept of compartmentation in brain energy metabolism gained new momentum with the postulation of the astrocyte neuron lactate shuttle model (ANLS). In the classical version of this hypothesis, glutamate transients are linked to a cellular compartmentation of lactate (Pellerin and Magistretti, 1994). Glutamate released from active neurons activates astrocytic glycolysis leading to production of lactate, which serves as an energy source for neurons. Increased brain lactate levels upon neuronal activation have been observed in several studies via different techniques (Hu and Wilson, 1997; Lin et al., 2010; Prichard et al., 1991; Sappey-Marinier et al., 1992). Also, L-lactate acts as a signaling molecule in certain mammalian brain regions (Mosienko et al., 2015; Tang et al., 2014; Yang et al., 2014). However, the cellular origin of lactate released during increased activity (Barros and Deitmer, 2010; Stobart and Anderson, 2013) and its significance as an energy substrate or signaling molecule remains largely unclear (Barros, 2013; Weber and Barros, 2015).

Experimental evidence from *in vitro* and *in vivo animal* studies demonstrate that lactate is able to sustain neuronal activity during glucose deprivation (Schurr, 2002; Wyss et al., 2011) and patients with non-penetrating traumatic brain injuries use peripheral lactate as brain energy substrates (for review see Glenn et al., 2015). Furthermore, lactate transport across cell membranes via monocarboxylate transporters (MCTs) is a facilitated transport (Halestrap and Wilson, 2012). Increased lactate production in one cell type and predominant lactate consumption in another cell type would therefore require a lactate concentration gradient from the 'producer' to the 'consumer'. Lactate dehydrogenase (LDH), located in mitochondria and the surrounding cytoplasm (Brooks et al., 1999), links lactate to oxidative metabolism, by catalyzing the conversion between lactate and pyruvate. The higher affinity

for lactate of MCT and LDH isoforms expressed in neurons (MCT2 and LDH1) relative to the isoforms expressed in astrocytes (MCT1/4 and LDH5) supports an astrocytic production and neuronal consumption of lactate (Bittar et al., 1996; Debernardi et al., 2003; Laughton et al., 2000; Pierre and Pellerin, 2005). Inhibition of astrocytic production and neuronal consumption of lactate via LDH inhibition reduces epileptic neuronal activity, possibly due to neuronal ATP depletion (Sada et al., 2015). Moreover, the fast and transient lactate depletion in astrocytes during different *in vivo* and *in vitro* stimulation paradigms may represent the emptying of a lactate pool (Sotelo-Hitschfeld et al., 2015). Taken together, these results suggest a lactate concentration gradient from astrocytes to neurons; however, *in vivo* evidence of such a cellular gradient is currently absent.

Here, we investigated cell-specific lactate reservoirs *in vivo* employing the recently developed genetically encoded biosensor *Laconic* (San Martín et al., 2013), which we specifically expressed in astrocytes and neurons. Through two-photon laser scanning microscopy (*2PLSM;* Denk et al., 1990), we show, for the first time, direct indication of an *in vivo* lactate gradient from astrocytes to neurons.

Results

Expression of *Laconic* and *Pyronic in vivo*

To evaluate the specificity of *Laconic* transients, a biosensor construct specific for pyruvate (‘*Pyronic’;* San Martín et al., 2014) was measured simultaneously with *Laconic*. Different adeno-associated viral (AAV) vectors, encoding either the *Laconic* or the *Pyronic* sensors, were injected in close distance to each other at the center of a craniotomy in the primary somatosensory cortex of mice (Figure 1A, S1A). The fluorescence of both sensors, driven by the short GFAP promoter, was located in the cytoplasm and showed the typical morphology of protoplasmic cortical astrocytes, including vascular end-feet and fine processes outlining dark non-fluorescent cells (Figure 1B). A similar fluorescence pattern was found throughout all imaged cortical layers, consistent with non-overlapping astrocytic domains in mice (Oberheim et al., 2009). Human synapsin promoter constructs induced cytoplasmic fluorescence in cells matching neuronal morphology, with dark nuclei and long ranging processes toward superficial or deeper structures, located more than 150 µm below the dura (Figure 1B). 2PLSM was restricted to layer 2/3 cells with a laser power above 20 mW to ensure stable FRET ratios (Figure S1F) and below 40 mW to prevent tissue damage and bleaching of the fluorescence. Immunohistochemical staining for GFAP, CD68 and fibrinogen revealed no increase in gliosis, microglial activity or blood-brain barrier leakage (Figures S1A-D).

Insert Figure 1 about here.

Laconic sensor functions are comparable *in vivo* and *in vitro*

L-lactate binding induces a conformational change of *Laconic* causing a decrease in fluorescent resonance energy transfer (FRET) efficiency which increases the ratio of mTFP (monomeric teal fluorescent protein) over Venus (Figure 1A). *In vitro* lactate application leads to two-site saturable *Laconic* kinetics without pH sensitivity (Figure 1C and S1F, San Martín et al., 2013). The functionality of the sensor *in vivo* was demonstrated with increasing doses of sodium-L-lactate injected via a tail vein

catheter during 2PLSM. *Laconic* signals in neurons and astrocytes increased non-linearly with the intravenously injected lactate dose but did not respond to 500 mM saline injections (Figure 2A, S1E). The amplitudes of *Laconic* signal changes *in vivo* were of the same order of magnitude as *in vitro* cell culture, where *Laconic* signals can be explored at a much wider range of lactate concentrations (Figure 2B).

Insert Figure 2 about here.

A single intravenous injection of lactate increases *Laconic* signal more in neurons than in astrocytes

To compare lactate accumulation in astrocytes and neurons, *Laconic* was simultaneously measured in neurons and astrocytes during short intravenous L-lactate infusions over three minutes (4 mmol/kg bodyweight), elevating blood lactate levels from 0.81 ± 0.26 mM to 17 ± 5.7 mM (Figure 3C). The *Laconic* signal increased more significantly in neurons than in astrocytes (5.7 ± 1.3% vs. 4.3 ± 1.3%, respectively; Figure 3A) with a rise in extracellular lactate levels of 0.27 ± 0.08 mM (Figure 3B). This discrepancy between neurons and astrocytes could reflect higher lactate accumulation in neurons at similar baseline lactate concentrations in both cell types. Alternatively, this difference could be attributed to lower baseline lactate concentrations in neurons, which would permit a greater upward dynamic range and sensitivity of *Laconic*. *Insert Figure 3 about here.*

To distinguish between these two possibilities, the baseline lactate concentrations in astrocytes and neurons were compared by saturating *Laconic* in both cellular compartments. Ammonium chloride infusion over four minutes (2.5 mmol/kg bodyweight), which boosts cytosolic lactate concentration in brain cells by inhibiting mitochondrial pyruvate consumption (Lerchundi et al., 2015), increased *Laconic* signals in neurons and astrocytes (7.3 ± 1.3% vs. 7.4 ± 1.6%, respectively; Figure S1H). When ammonium chloride and L-lactate were simultaneously infused intravenously beforehand, additional L-lactate application induced a significantly smaller increase of the *Laconic* signal in neurons (0.95 ± 0.62%, n = 53, $p < 0.05$, one-sample t-test) and astrocytes (0.57 ± 0.55%, n = 43 cells, $p < 0.05$, one-

sample t-test) (Figure 4A) compared to the same lactate infusion in Figure 3 ($p < 10^{-7}$, two-sample t-test). However, extracellular lactate levels continued to increase with additional lactate infusion by 16 ± 10.7% of the total increase ($p < 0.05$, one-sample t-test) (Figure 4B). This suggests that ammonium chloride administration increased intracellular lactate concentrations to levels which saturated *Laconic*. Overall, a greater change in neuronal *Laconic* signal was observed (ΔFRET signal: 9.9 ± 2.4 %) compared to astrocytes (6.9 ± 2.0 %), supporting our hypothesis of lower baseline lactate levels in neurons (Figure 4A).

Insert Figure 4 about here.

Pronounced trans-acceleration in astrocytes occurs at baseline

Pyruvate application has been used *in vitro* to decrease intracellular lactate levels in erythrocytes (Fishbein et al., 1988). This effect is based on a property of MCTs called trans-acceleration (Figure 5E), where the presence of extracellular monocarboxylates stimulates transporter substrate efflux. This process involves a facilitated conformational switch of the substrate binding site across the cell membrane when an adequate substrate is bound (Figure S2G, Garcia et al., 1994; Halestrap, 2013).

To test the capacity of intravenously applied pyruvate to produce a trans-acceleration-induced lactate efflux out of brain cells, extracellular brain lactate levels were measured with Pinnacle© biosensors (Figure S3D). Intravenous injection of 4 mmol/kg pyruvate over three minutes induced a transient increase of extracellular lactate levels of 0.084 ± 0.022 mM (Figure 5B), consistent with trans-acceleration of MCTs.

To compare trans-acceleration of MCTs in neurons and astrocytes, simultaneous measurements of *Laconic* and *Pyronic* during pyruvate application were performed. At baseline lactate levels, pyruvate decreased *Laconic* signal in astrocytes (-4.7 ± 1.5%), while signal in neurons was relatively unchanged (-0.6 ± 0.9%; Figure 5A). *Pyronic* showed only minor changes. However, after achieving higher intracellular lactate concentrations by the combined infusion of ammonium chloride and lactate, pyruvate administration was able to decrease *Laconic* signals in both astrocytes and neurons while

increasing *Pyronic* signals in both cells (Figure 5C). Upon repeated i.v. injections of pyruvate, neuronal Laconic signal kept increasing, possibly due to the conversion of pyruvate to lactate (Gonzalez et al., 2005). Under these high lactate conditions, both astrocytes and neurons show trans-acceleration (Figure 5D), demonstrating that neuronal MCTs are also susceptible to pyruvate-driven efflux (Figure 5E). In a subset of recordings this lactate accumulation was absent in neurons, in which case a lactate depletion during pyruvate infusions could not be observed.

Insert Figure 5 about here.

Discussion

The compartmentation of brain energy metabolism is a subject of intense debate, fuelled by a lack of accurate *in vivo* intracellular lactate measurements in different cell populations. Here, we utilized the genetically encoded lactate sensor *Laconic* to observe the capacity of blood borne lactate to enter both astrocytes and neurons and to approximate lactate concentrations in these cells. Whole brain tissue uptake of lactate from blood has previously been demonstrated *in vivo* (Cremer et al., 1979; Klein and Olsen, 1947; Wyss et al., 2011) and has been quantified in humans (Glenn et al., 2015; van Hall et al., 2009). We observed an accumulation of cellular and extracellular brain lactate during artificially increased blood lactate levels, which indicate a net uptake under these conditions and is in agreement with findings in humans (Boumezbeur et al., 2010; Quistorff et al., 2008; Rasmussen et al., 2011). The ability of neurons to take up lactate is an important prerequisite for the use of lactate as an energy substrate as suggested by the ANLS (Bélanger et al., 2011; Magistretti and Allaman, 2015), a concept that is still debated (Dienel, 2012 and references therein). Lactate has been shown to enter oxidative energy production in physiological resting conditions (Bouzier-Sore et al., 2006) and support neuronal activity under low-glucose conditions both *in vitro* (Tekkök et al., 2005) and *in vivo* (Herzog et al., 2013; Wyss et al., 2011).

We observed a greater neocortical *Laconic* signal increase in neurons than in astrocytes when blood lactate was elevated. This cell type difference was not due to altered *Laconic* sensitivity, as cumulative signal amplitudes were similar in both populations after decreasing intracellular lactate with pyruvate infusions and normalizing to the saturated sensor (Figure S1I). Therefore, baseline neuronal lactate levels could be lower where *Laconic* is more responsive. To evaluate this possibility, *Laconic* was saturated in both cellular compartments simultaneously using a mixture of lactate and ammonium (Provent et al., 2007), which revealed a higher maximal increase of neuronal *Laconic* and suggests a lower baseline lactate concentration in neurons than in astrocytes (Figure 6A).

We utilized the trans-acceleration property of MCTs (Brown and Brooks, 1994) by applying an inward pyruvate gradient to force the cells to release their lactate. The pronounced drop of astrocytic lactate and the negligible decrease in neurons is in agreement with higher resting lactate levels in astrocytes (Figure 6B). We can reject the following alternative explanations for the astrocyte-specific lactate drop: First, cell-type specific expression of isoforms in the brain has been reported with MCT1 mainly expressed in astrocytes and oligodendrocytes and MCT2 in neurons (Pellerin et al., 2005). We assessed the influence of MCT isoforms on trans-acceleration with a numerical model and demonstrated an almost linear dependency of the pyruvate-induced trans-acceleration on intracellular baseline lactate levels for both MCT1 and MCT2 (Figure S2A-C). However, the relatively higher affinity of MCT2 than MCT1 for pyruvate in our model would predict stronger trans-acceleration of MCT2, i.e. in neurons (Figure S2A-C). Also, trans-acceleration can be induced in cultured neurons (Figure S2E) and astrocytes (Figure S2F), where baseline lactate levels depend on the experimental conditions. The differential MCT isoform expression and kinetics can therefore not explain the predominant trans-acceleration in astrocytes.

Second, LDH diminishes lactate depletion caused by pyruvate uptake over time by transforming pyruvate into lactate. Intracellular lactate levels start to increase during pyruvate exposure if the rate of LDH-catalyzed conversion of pyruvate to lactate is high compared to lactate transport (Figure S2C) which may explain the delayed increase in lactate we observed following pyruvate infusion (Figure 5A).

However, the lower NADH/NAD+ ratio in neurons compared to astrocytes (Hung et al., 2011) implies weaker conversion of pyruvate to lactate and is therefore unlikely to mask pyruvate induced lactate depletion in neurons.

Third, the brain vasculature is almost entirely covered by astrocytic endfeet (Mathiisen et al., 2010; McCaslin et al., 2011). Therefore, astrocytes are predominantly exposed to blood-borne pyruvate. The main transport limiting barrier for blood-borne pyruvate to enter brain tissue is MCT1 at the endothelial membranes and the fast diffusion within the tissue will expose all brain cells similarly (Halestrap, 2013; Miller and Oldendorf, 1986). Accordingly, we did not observe any temporal differences between astrocytic and neuronal lactate accumulation (Figure 2A and 3A). Additionally, buffering of lactate by *Laconic* is unlikely, because baseline lactate levels are higher (hundreds of µM instead of nM) and lactate transients are slower (multiple seconds instead of ms) than in the case of calcium dynamics, where buffering by the sensor is reported to be an issue (Grienberger and Konnerth, 2012). Finally, increasing lactate levels in neurons lead to trans-acceleration and lactate efflux in neurons similarly as in astrocytes (Figure 5C-D).

A higher resting state lactate level in astrocytes in comparison to neurons has significant implications for transcellular lactate exchange. Intracellular lactate accumulation driven by increased blood lactate and depletion during increased blood pyruvate is consistent with a facilitated transport of lactate via MCTs. The direction of a facilitated transport is determined by the concentration gradient, for which we found evidence to be from astrocytes to neurons as has been suggested by the ANLS (Pellerin and Magistretti, 1994) (Figure 6A). However, alternative lactate transport mechanisms have been suggested, such as via pannexins and connexins (Barros, 2013; Giaume et al., 2013) or an unknown potassium-dependent ion channel, which would allow active lactate transport even against a chemical concentration gradient during increased neuronal activity (Sotelo-Hitschfeld et al., 2015).

In addition, astrocytic lactate could provide a small but fast energy reserve; cultured astrocytes have been shown to preferentially export glucose-derived lactate rather than lactate derived from glycogen (Sickmann et al., 2005). Glycogen may serve as a slower energy pool, as astrocytic glycogen-derived

lactate sustains neuronal function in rat optical nerve preparations for several minutes (Brown and Ransom, 2007).

Our data provide important information about lactate concentrations of the different cellular compartments, which are fundamental for the role of lactate as an activity dependent signaling molecule (Mosienko et al., 2015). The transport of lactate from astrocytes to neurons has been shown to be necessary for the establishment of long-term memory (Suzuki et al., 2011) by inducing the expression of plasticity-related genes (Yang et al., 2014). Volatile halogenated anesthetics such as isoflurane are known to increase brain lactate levels (Boretius et al., 2013; Horn and Klein, 2010) and Fünfschilling and colleagues (Fünfschilling et al., 2012) reported a marked decrease in tissue lactate concentration in response to the discontinuation of isoflurane anesthesia, indicative of a substantial lactate exchange. In our study, we used injectable anesthetics to avoid elevated lactate levels, but our results can be used to interpret the direction of isoflurane-induced lactate exchange at the cellular level. It is important to note, however, that *Laconic* did not enable us to measure cellular or whole brain lactate transport or oxidation rates *in vivo*, as currently available pharmacological agents (such as the MCT blocker α-cyano-4-hydroxycinnamate) are neither fast (seconds) nor specific (limited side effects) enough. *Insert Figure 6 about here.*

In summary, the genetically encoded lactate sensor *Laconic* in combination with 2PLSM was successfully applied to investigate brain energy metabolism at the single cell level *in vivo* for the first time. We demonstrate that neurons and astrocytes readily take up blood-borne lactate. Our data suggest a significantly lower baseline lactate level in neurons in comparison to astrocytes. Our findings furthermore support the concept of compartmentalized lactate pools with a lactate flux from astrocytes to neurons.

Experimental Procedures

Viral constructs of the lactate sensor *Laconic* and the pyruvate sensor *Pyronic*

Genetically-encoded FRET sensors for lactate (‘*Laconic’;* San Martín et al., 2013), and pyruvate (‘*Pyronic’*; San Martín et al., 2014), were cloned into adeno-associated viral (AAV) plasmids for astrocyte and neuron specific expression. The astrocyte-specific construct included a minimal GFAP promoter ($GfaABC_1D$, sGFAP; kindly provided by Dr. M. Brenner, Department of Neurobiology, University of Alabama) (Lee et al., 2008), a beta-globin intron, and a poly-adenylation signal. The neuronal construct included a human synapsin-1 (SYN) promoter, a Woodchuck Hepatitis Virus (WHP) Post-transcriptional Regulatory Element (WPRE) and a poly-adenylation signal (Glover et al., 2002; Kügler et al., 2001). The four different shuttle plasmids (pAAV-SYN-*Laconic*, pAAV-GFAP-*Laconic*, pAAV-SYN-*Pyronic*, and pAAV-GFAP-*Pyronic*) were used to generate AAV serotype 6 (SYN constructs) or AAV serotype 9 (GFAP constructs) viral particles, by co-transfecting the shuttle plasmid with the pDP6 and pDF9 helper plasmids in HEK293-AAV cells (Agilent Technologies, Santa Clara, CA). Viral particles were isolated from the cell lysates, using iodixanol step gradients and HPLC purification on heparin-binding (AAV6) and ion exchange (AAV9) columns. The number of viral genomic copies (VG) was measured by TaqMan real-time PCR, with primers amplifying specific sequences in the human beta-globin intron or WPRE element.

Animals

All experimental procedures were approved by the local veterinary authorities in Zurich and conformed to the guidelines of the Swiss Animal Protection Law, Veterinary Office, Canton of Zurich (Act of Animal Protection 16 December 2005 and Animal Protection Ordinance 23 April 2008). Surgery was performed in female wild type mice (*C57BL/6J*; Charles River) of 8 to 10 weeks of age (20 to 25 gram bodyweight). The mice had free access to water and food and an inverted 12-hour light/dark cycle.

Anesthesia

The animals were anesthetized with a mixture of fentanyl (0.05 mg per kg bodyweight; *Sintenyl,* Sintetica, Switzerland), midazolam (5 mg per kg bodyweight; *Dormicum*, Roche, Switzerland) and

medetomidine (0.5 mg per kg bodyweight; *Domitor*, Orion Pharma, Finland) intraperitoneally and anesthesia was maintained with midazolam (5 mg per kg bodyweight) subcutaneously after 50 minutes. To prevent hypoxaemia, a face mask provided 300 mL/min of 100% oxygen. Core temperature was kept constant at 37°C using a homeothermic blanket heating system during all surgical and experimental procedures (Harvard Apparatus, Holliston, MA, USA). The head was fixed in a stereotaxic apparatus and the eyes were kept wet with ointment (vitamin A eye cream; Bausch & Lomb, Switzerland).

Virus injection

A 4x4 mm craniotomy was performed above the somatosensory cortex using a dental drill (Bien-Air, Bienne, Switzerland) and solutions containing virus vector were injected into the primary somatosensory cortex at a close distance to achieve neighboring, but non-overlapping, sensor protein expression: 75 nL of AAV9-GFAP-*Laconic* (titer 3.1E12 VG/mL); 150 nL of AAV6-SYN-*Laconic* (titer 1.02E13 VG/mL) (San Martín et al., 2013); 75 nL of AAV9-GFAP-*Pyronic* (titer 1.6E12 VG/mL); 150 nL of AAV6-SYN-*Pyronic* (titer 1.15E12 VG/mL) (San Martín et al., 2014). Large vessels were avoided to prevent bleeding and the absorption of light by hemoglobin during imaging. A square cover slip (3x3 mm, UQG Optics Ltd, UK) was placed on the exposed dura mater and fixed to the skull with dental cement, according to published protocols (Holtmaat et al., 2009).

Head-post implantation

A bonding agent (*Gluma Comfort Bond*; Heraeus Kulzer, Hanau, Germany) was applied to the cleaned skull and polymerized with a handheld blue light source (600 mW/cm^2; Demetron LC, Switzerland). A custom-made aluminium head post was connected with dental cement (*EvoFlow*; Ivoclar Vivadent AG, Liechtenstein) to the bonding agent for later reproducible animal fixation in the microscopic setup. The skin lesion was treated with antibiotic ointment (Neomycin, *Cicatrex*; Janssen-Cilag AG, Switzerland) and closed with acrylic glue (*Histoacryl*, B. Braun, Germany). After surgery the animals were kept warm and provided with analgesics (metamizole 0.2 mg/g bodyweight; Sintetica, Switzerland) and an

antibiotic was added to the drinking water (enrofloxacin, 200 mg/l drinking water; *Baytril*, Bayer, Germany). Sensor protein expression was checked using a fluorescence stereomicroscope (*Leica MZ16 FA*) two to three weeks after virus injection and prior to imaging.

Intracellular lactate measurements

The mice were imaged using a custom-built two-photon laser scanning microscope (2PLSM) with a tunable pulsed laser (*MaiTai eHP DS* system, Spectra-Physics, CA, USA) at 870 nm wavelength and equipped with a 20x water immersion objective (W-Plan-Apochromat 20x/1.0 differential interference contrast, Zeiss, Germany). During measurements the animals were head-fixed and kept under the anesthesia described above. The galvo-mirrors and a motorized objective were used to cycle through two to four individual fields of view. Unidirectional frame scans at 0.1 Hz and 512x512 pixels resolution were acquired with *ScanImage* (r3.8.1; Janelia Research Campus; Pologruto et al., 2003)). Lactate concentration in cultured cells were measured with the use of *Laconic* as previously described (Sotelo-Hitschfeld et al., 2015).

Extracellular lactate measurements

Extracellular lactate measurements were performed with a commercially available recording system (*Pinnacle Inc.*, Lawrence, KS, USA). Mice were fixed in a stereotactic frame under anesthesia (isoflurane 1.5%; Abbott, North Chicago, IL, USA), the skull was opened with a dental drill, and a guide cannula (Part 7032, Pinnacle Technology, Lawrence, KS, USA) was implanted into the primary somatosensory cortex (from bregma: A/P +1.41, M/L -2.8, D/V -1.0) and fixed with dental cement to an anchor screw (Part 8209, Pinnacle Technology, Lawrence, KS, USA). After a recovery period of two weeks, the pre-calibrated lactate biosensor was inserted into the guide cannula (Naylor et al., 2012). A tail vein catheter was inserted for saline, lactate and pyruvate infusions. Recording started after one hour of signal stabilization.

Blood lactate level measurements

The femoral artery was exposed and cannulated with fine bore polyethylene tubing (0.28 mm ID, 0.61 mm OD, Portex, Smith medical, UK) to measure blood lactate level. Blood drops were removed from the cannula and every fourth drop was used for an enzymatic lactate assay (*Lactate Pro 2*, Arkray, Japan). After each blood sample analysis, the tubing was rinsed with heparinized (50 IU/ml) 0.9% saline solution.

Intervention protocols

For intravenous interventions, a 30 Gauge needle was connected to fine bore polyethylene tubing (0.28 mm ID, 0.61 mm OD, Portex, Smith medical, UK), filled with 0.9% saline solution and inserted into one of the tail veins. Before imaging, the tubing was connected via an X connector (model *SC25*, Instech, USA) to peristaltic pumps (*Reglo digital ISM 831*, Ismatec SA, Germany), which were operated via custom written *Matlab* codes. A 500 mM solution of sodium chloride (*S7653*, Sigma-Aldrich, MO, USA), sodium L-lactate (*L7022*, Sigma, MO, USA) or sodium pyruvate (*P2256*, Sigma-Aldrich, MO, USA) at 4 mmol per kg bodyweight was injected during 3 minutes.

Immunohistochemistry

Four mice expressing astrocytic and neuronal *Laconic* sensors and one mouse intraperitoneally injected with 2 mg per kg bodyweight lipopolysaccharides (Fontana et al., 1981) were anesthetized with pentobarbital (*Nembutal*, >50 mg/kg) intraperitoneally and transcardially perfused with 2% paraformaldehyde to assess immunohistochemical alterations. Brains were post-fixed in 4% paraformaldehyde, rinsed with phosphate-buffered saline (PBS), and cryoprotected with 30 % sucrose in PBS. The frozen brains were then cut into 40 µm sections with a sliding microtome and fluorescent regions were identified with a fluorescence stereomicroscope (*Leica MZ16 FA*; Leica Microsystems, Germany). Free-floating sections were incubated with rabbit anti-Glial fibrillary acidic protein (GFAP) antibody (*Z0334*; DakoCytomation, DK), rabbit anti-fibrinogen antibody (*A0080*; DakoCytomation, DK) or rat anti-CD68 antibody (*MCA1957GA*; AbD Serotec) and stained with red-fluorescent secondary antibody (goat anti-rabbit and goat anti-rat Cy3; Jackson Immuno Research Laboratories Inc.). Images

of the sections were collected with a laser-scanning confocal microscope (*LSM510-Meta*; Zeiss, Germany).

Cell culture experiments

All animal procedures for the *cell culture* experiments were approved by the *Institutional Animal Care and Use Committee* of the *Centro de Estudios Científicos*. Mixed cortical cultures of neuronal and glial cells were prepared from 1-3 day-old neonates (*C57BL/6J*) as detailed previously (Bittner, 2010). For *Laconic* sensor expression, cultures were exposed to 5 x 10^6 PFU of *Ad Laconic* and studied after 48 h (culture day 8-10). The co-culture cells were imaged with an upright *Olympus FV1000* confocal microscope and a 440 nm solid-state laser as detailed previously (Sotelo-Hitschfeld et al., 2015). Masked ratio images were generated from background-subtracted images using *ImageJ* software.

Data analysis and statistics

Astrocytic domains and neuronal cytoplasm of individual cells of cortical layers L2/3 (150-250 µm below the dura) were outlined using ImageJ (1.46r; National Institutes of Health, USA). The mTFP channel (with bandpass filter 475/64; Semrock, USA) was divided by the Venus channel (with bandpass filter 542/50; Semrock, USA) and the ratio was normalized to the corresponding baseline or as indicated in the figure legend using Matlab (MathWorks, USA). Time acquisition curves are filtered with a moving average of five frames and indicated as mean ± standard deviation. Effects in multiple animals were compared using t-tests in R (R Core Team, 2014). P values < 0.05 were taken as significance limit.

Author contributions

P.M. performed the in vivo two-photon experiments. M.E. and P.M. performed the extracellular lactate measurements. P.M., A.F.C., V.K., M.T.W., R.G. and M.Z. helped establish in vivo and in vitro experimental protocols. I.R.-G. and F.B.-L. performed cell culture experiments. A.S.M. and F.B. created the sensors *Laconic* and *Pyronic*. J.S., S.L. and B.S. prepared the viral vectors. P.M., M.T.W., F.B, J.S. and B.W. wrote the manuscript. P.M., M.T.W., P.J.M., F.B. and B.W. conceived and designed experiments. P.A., P.J.M., F.B. and B.W. provided laboratory infrastructure and financial support. All authors discussed the data and critically revised the manuscript.

Acknowledgements

This research was partly supported by the Swiss National Science Foundation, the Hartmann Müller-Stiftung, and the Swiss Foundation for Excellence in Biomedical Research. BW is a member of the Clinical Research Priority Program of the University of Zurich on Molecular Imaging. LFB is partly funded by the Fondecyt Grant 1130095. The Centro de Estudios Científicos CECs is funded by the Chilean Government through the Centers of Excellence Basal Financing Program of CONICYT.

References

Barros, L.F. (2013). Metabolic signaling by lactate in the brain. Trends Neurosci. *36*, 396–404.

Barros, L.F., and Deitmer, J.W. (2010). Glucose and lactate supply to the synapse. Brain Res. Rev. *63*, 149–159.

Bélanger, M., Allaman, I., and Magistretti, P.J. (2011). Brain Energy Metabolism: Focus on Astrocyte-Neuron Metabolic Cooperation. Cell Metab. *14*, 724–738.

Van den Berg, C.J., Krzalić, L., Mela, P., and Waelsch, H. (1969). Compartmentation of glutamate metabolism in brain. Evidence for the existence of two different tricarboxylic acid cycles in brain. Biochem. J. *113*, 281–290.

Bittar, P.G., Charnay, Y., Pellerin, L., Bouras, C., and Magistretti, P.J. (1996). Selective Distribution of Lactate Dehydrogenase Isoenzymes in Neurons and Astrocytes of Human Brain. J. Cereb. Blood Flow Metab. *16*, 1079–1089.

Bittner, C.X. (2010). High resolution measurement of the glycolytic rate. Front. Neuroenergetics *2*.

Boretius, S., Tammer, R., Michaelis, T., Brockmöller, J., and Frahm, J. (2013). Halogenated volatile anesthetics alter brain metabolism as revealed by proton magnetic resonance spectroscopy of mice in vivo. NeuroImage *69*, 244–255.

Boumezbeur, F., Petersen, K.F., Cline, G.W., Mason, G.F., Behar, K.L., Shulman, G.I., and Rothman, D.L. (2010). The Contribution of Blood Lactate to Brain Energy Metabolism in Humans Measured by Dynamic 13C Nuclear Magnetic Resonance Spectroscopy. J. Neurosci. *30*, 13983–13991.

Bouzier-Sore, A.-K., Voisin, P., Bouchaud, V., Bezancon, E., Franconi, J.-M., and Pellerin, L. (2006). Competition between glucose and lactate as oxidative energy substrates in both neurons and astrocytes: a comparative NMR study. Eur. J. Neurosci. *24*, 1687–1694.

Brooks, G.A., Dubouchaud, H., Brown, M., Sicurello, J.P., and Butz, C.E. (1999). Role of mitochondrial lactate dehydrogenase and lactate oxidation in the intracellular lactate shuttle. Proc. Natl. Acad. Sci. *96*, 1129–1134.

Brown, A.M., and Ransom, B.R. (2007). Astrocyte glycogen and brain energy metabolism. Glia *55*, 1263–1271.

Brown, M.A., and Brooks, G.A. (1994). Trans-Stimulation of Lactate Transport from Rat Sarcolemmal Membrane Vesicles. Arch. Biochem. Biophys. *313*, 22–28.

Cremer, J.E., Cunningham, V.J., Pardridge, W.M., Braun, L.D., and Oldendorf, W.H. (1979). Kinetics of Blood-Brain Barrier Transport of Pyruvate, Lactate and Glucose in Suckling, Weanling and Adult Rats. J. Neurochem. *33*, 439–445.

Debernardi, R., Pierre, K., Lengacher, S., Magistretti, P.J., and Pellerin, L. (2003). Cell-specific expression pattern of monocarboxylate transporters in astrocytes and neurons observed in different mouse brain cortical cell cultures. J. Neurosci. Res. *73*, 141–155.

Denk, W., Strickler, J.H., and Webb, W.W. (1990). Two-photon laser scanning fluorescence microscopy. Science *248*, 73–76.

Dienel, G.A. (2012). Brain lactate metabolism: the discoveries and the controversies. J. Cereb. Blood Flow Metab. *32*, 1107–1138.

Fishbein, W.N., Foellmer, J.W., Davis, J.I., Fishbein, T.M., and Armbrustmacher, P. (1988). Clinical assay of the human erythrocyte lactate transporter: I. Principles, procedure, and validation. Biochem. Med. Metab. Biol. *39*, 338–350.

Fontana, A., Bosshard, R., Dahinden, C., Grob, P., and Grieder, A. (1981). Glia cell response to bacterial lipopolysaccharide: Effect on nucleotide synthesis, its genetic control and definition of the active principle. J. Neuroimmunol. *1*, 343–352.

Fünfschilling, U., Supplie, L.M., Mahad, D., Boretius, S., Saab, A.S., Edgar, J., Brinkmann, B.G., Kassmann, C.M., Tzvetanova, I.D., Möbius, W., et al. (2012). Glycolytic oligodendrocytes maintain myelin and long-term axonal integrity. Nature *485*, 517–521.

Garcia, C.K., Goldstein, J.L., Pathak, R.K., Anderson, R.G.W., and Brown, M.S. (1994). Molecular characterization of a membrane transporter for lactate, pyruvate, and other monocarboxylates: Implications for the Cori cycle. Cell *76*, 865–873.

Giaume, C., Leybaert, L., C. Naus, C., and C. Sáez, J. (2013). Connexin and pannexin hemichannels in brain glial cells: properties, pharmacology, and roles. Front. Pharmacol. *4*.

Glenn, T.C., Martin, N.A., Horning, M.A., McArthur, D.L., Hovda, D.A., Vespa, P., and Brooks, G.A. (2015). Lactate: Brain Fuel in Human Traumatic Brain Injury: A Comparison with Normal Healthy Control Subjects. J. Neurotrauma *32*, 820–832.

Glover, C.P.J., Bienemann, A.S., Heywood, D.J., Cosgrave, A.S., and Uney, J.B. (2002). Adenoviral-Mediated, High-Level, Cell-Specific Transgene Expression: A SYN1-WPRE Cassette Mediates Increased Transgene Expression with No Loss of Neuron Specificity. Mol. Ther. *5*, 509–516.

Gonzalez, S.V., Nguyen, N.H.T., Rise, F., and Hassel, B. (2005). Brain metabolism of exogenous pyruvate. J. Neurochem. *95*, 284–293.

Grienberger, C., and Konnerth, A. (2012). Imaging Calcium in Neurons. Neuron *73*, 862–885.

Halestrap, A.P. (2013). Monocarboxylic acid transport. Compr. Physiol. *3*, 1611–1643.

Halestrap, A.P., and Wilson, M.C. (2012). The monocarboxylate transporter family—Role and regulation. IUBMB Life *64*, 109–119.

van Hall, G., Stromstad, M., Rasmussen, P., Jans, O., Zaar, M., Gam, C., Quistorff, B., Secher, N.H., and Nielsen, H.B. (2009). Blood lactate is an important energy source for the human brain. J Cereb Blood Flow Metab *29*, 1121–1129.

Herzog, R.I., Jiang, L., Herman, P., Zhao, C., Sanganahalli, B.G., Mason, G.F., Hyder, F., Rothman, D.L., Sherwin, R.S., and Behar, K.L. (2013). Lactate preserves neuronal metabolism and function following antecedent recurrent hypoglycemia. J. Clin. Invest. *123*, 1988–1998.

Holtmaat, A., Bonhoeffer, T., Chow, D.K., Chuckowree, J., De Paola, V., Hofer, S.B., Hübener, M., Keck, T., Knott, G., Lee, W.-C.A., et al. (2009). Long-term, high-resolution imaging in the mouse neocortex through a chronic cranial window. Nat. Protoc. *4*, 1128–1144.

Horn, T., and Klein, J. (2010). Lactate levels in the brain are elevated upon exposure to volatile anesthetics: A microdialysis study. Neurochem. Int. *57*, 940–947.

Hu, Y., and Wilson, G.S. (1997). A Temporary Local Energy Pool Coupled to Neuronal Activity: Fluctuations of Extracellular Lactate Levels in Rat Brain Monitored with Rapid-Response Enzyme-Based Sensor. J. Neurochem. *69*, 1484–1490.

Hung, Y.P., Albeck, J.G., Tantama, M., and Yellen, G. (2011). Imaging Cytosolic NADH-NAD+ Redox State with a Genetically Encoded Fluorescent Biosensor. Cell Metab. *14*, 545–554.

Klein, J.R., and Olsen, N.S. (1947). Distribution of Intravenously Injected Glutamate, Lactate, Pyruvate, and Succinate Between Blood and Brain. J. Biol. Chem. *167*, 1–5.

Kügler, S., Meyn, L., Holzmüller, H., Gerhardt, E., Isenmann, S., Schulz, J.B., and Bähr, M. (2001). Neuron-Specific Expression of Therapeutic Proteins: Evaluation of Different Cellular Promoters in Recombinant Adenoviral Vectors. Mol. Cell. Neurosci. *17*, 78–96.

Laughton, J.D., Charnay, Y., Belloir, B., Pellerin, L., Magistretti, P.J., and Bouras, C. (2000). Differential messenger RNA distribution of lactate dehydrogenase LDH-1 and LDH-5 isoforms in the rat brain. Neuroscience *96*, 619–625.

Lee, Y., Messing, A., Su, M., and Brenner, M. (2008). GFAP promoter elements required for region-specific and astrocyte-specific expression. Glia *56*, 481–493.

Lerchundi, R., Fernández-Moncada, I., Contreras-Baeza, Y., Sotelo-Hitschfeld, T., Mächler, P., Wyss, M.T., Stobart, J., Baeza-Lehnert, F., Alegría, K., Weber, B., et al. (2015). NH4+ triggers the release of astrocytic lactate via mitochondrial pyruvate shunting. Proc. Natl. Acad. Sci. 201508259.

Lin, A.-L., Fox, P.T., Hardies, J., Duong, T.Q., and Gao, J.-H. (2010). Nonlinear coupling between cerebral blood flow, oxygen consumption, and ATP production in human visual cortex. Proc. Natl. Acad. Sci. *107*, 8446–8451.

Magistretti, P.J., and Allaman, I. (2015). A Cellular Perspective on Brain Energy Metabolism and Functional Imaging. Neuron *86*, 883–901.

Martinez-Hernandez, A., Bell, K.P., and Norenberg, M.D. (1977). Glutamine Synthetase: Glial Localization in Brain. Science *195*, 1356–1358.

Mathiisen, T.M., Lehre, K.P., Danbolt, N.C., and Ottersen, O.P. (2010). The perivascular astroglial sheath provides a complete covering of the brain microvessels: An electron microscopic 3D reconstruction. Glia *58*, 1094–1103.

McCaslin, A.F.H., Chen, B.R., Radosevich, A.J., Cauli, B., and Hillman, E.M.C. (2011). In vivo 3D morphology of astrocyte-vasculature interactions in the somatosensory cortex: implications for neurovascular coupling. J. Cereb. Blood Flow Metab. *31*, 795–806.

Miller, L.P., and Oldendorf, W.H. (1986). Regional Kinetic Constants for Blood–Brain Barrier Pyruvic Acid Transport in Conscious Rats by the Monocarboxylic Acid Carrier. J. Neurochem. *46*, 1412–1416.

Mosienko, V., Teschemacher, A.G., and Kasparov, S. (2015). Is L-lactate a novel signaling molecule in the brain? J. Cereb. Blood Flow Metab. *35*, 1069–1075.

Naylor, E., Aillon, D.V., Barrett, B.S., Wilson, G.S., Johnson, D.A., Johnson, D.A., Harmon, H.P., Gabbert, S., and Petillo, P.A. (2012). Lactate as a Biomarker for Sleep. Sleep *35*, 1209–1222.

Oberheim, N.A., Takano, T., Han, X., He, W., Lin, J.H.C., Wang, F., Xu, Q., Wyatt, J.D., Pilcher, W., Ojemann, J.G., et al. (2009). Uniquely Hominid Features of Adult Human Astrocytes. J. Neurosci. *29*, 3276–3287.

Pellerin, L., and Magistretti, P.J. (1994). Glutamate uptake into astrocytes stimulates aerobic glycolysis: a mechanism coupling neuronal activity to glucose utilization. Proc. Natl. Acad. Sci. *91*, 10625–10629.

Pellerin, L., Bergersen, L.H., Halestrap, A.P., and Pierre, K. (2005). Cellular and subcellular distribution of monocarboxylate transporters in cultured brain cells and in the adult brain. J. Neurosci. Res. *79*, 55–64.

Pierre, K., and Pellerin, L. (2005). Monocarboxylate transporters in the central nervous system: distribution, regulation and function. J. Neurochem. *94*, 1–14.

Pologruto, T.A., Sabatini, B.L., and Svoboda, K. (2003). ScanImage: Flexible software for operating laser scanning microscopes. Biomed. Eng. OnLine *2*, 13.

Prichard, J., Rothman, D., Novotny, E., Petroff, O., Kuwabara, T., Avison, M., Howseman, A., Hanstock, C., and Shulman, R. (1991). Lactate rise detected by 1H NMR in human visual cortex during physiologic stimulation. Proc. Natl. Acad. Sci. *88*, 5829–5831.

Provent, P., Kickler, N., Barbier, E.L., Bergerot, A., Farion, R., Goury, S., Marcaggi, P., Segebarth, C., and Coles, J.A. (2007). The ammonium-induced increase in rat brain lactate concentration is rapid and reversible and is compatible with trafficking and signaling roles for ammonium. J. Cereb. Blood Flow Metab. *27*, 1830–1840.

Quistorff, B., Secher, N.H., and Lieshout, J.J.V. (2008). Lactate fuels the human brain during exercise. FASEB J. *22*, 3443–3449.

Rasmussen, P., Wyss, M.T., and Lundby, C. (2011). Cerebral glucose and lactate consumption during cerebral activation by physical activity in humans. FASEB J. *25*, 2865–2873.

R Core Team (2014). R: A Language and Environment for Statistical Computing (Vienna, Austria: R Foundation for Statistical Computing).

Sada, N., Lee, S., Katsu, T., Otsuki, T., and Inoue, T. (2015). Targeting LDH enzymes with a stiripentol analog to treat epilepsy. Science *347*, 1362–1367.

San Martín, A., Ceballo, S., Ruminot, I., Lerchundi, R., Frommer, W.B., and Barros, L.F. (2013). A Genetically Encoded FRET Lactate Sensor and Its Use To Detect the Warburg Effect in Single Cancer Cells. PLoS ONE *8*, e57712.

San Martín, A., Ceballo, S., Baeza-Lehnert, F., Lerchundi, R., Valdebenito, R., Contreras-Baeza, Y., Alegría, K., and Barros, L.F. (2014). Imaging Mitochondrial Flux in Single Cells with a FRET Sensor for Pyruvate. PLoS ONE *9*, e85780.

Sappey-Marinier, D., Calabrese, G., Fein, G., Hugg, J.W., Biggins, C., and Weiner, M.W. (1992). Effect of Photic Stimulation on Human Visual Cortex Lactate and Phosphates Using 1H and 31P Magnetic Resonance Spectroscopy. J. Cereb. Blood Flow Metab. *12*, 584–592.

Schurr, A. (2002). Lactate, glucose and energy metabolism in the ischemic brain (Review). Int. J. Mol. Med. *10*, 131–136.

Sickmann, H.M., Schousboe, A., Fosgerau, K., and Waagepetersen, H.S. (2005). Compartmentation of Lactate Originating from Glycogen and Glucose in Cultured Astrocytes. Neurochem. Res. *30*, 1295–1304.

Sotelo-Hitschfeld, T., Niemeyer, M.I., Mächler, P., Ruminot, I., Lerchundi, R., Wyss, M.T., Stobart, J., Fernández-Moncada, I., Valdebenito, R., Garrido-Gerter, P., et al. (2015). Channel-Mediated Lactate Release by K+-Stimulated Astrocytes. J. Neurosci. *35*, 4168–4178.

Stobart, J.L., and Anderson, C.M. (2013). Multifunctional role of astrocytes as gatekeepers of neuronal energy supply. Front. Cell. Neurosci. *7*.

Suzuki, A., Stern, S.A., Bozdagi, O., Huntley, G.W., Walker, R.H., Magistretti, P.J., and Alberini, C.M. (2011). Astrocyte-Neuron Lactate Transport Is Required for Long-Term Memory Formation. Cell *144*, 810–823.

Tang, F., Lane, S., Korsak, A., Paton, J.F.R., Gourine, A.V., Kasparov, S., and Teschemacher, A.G. (2014). Lactate-mediated glia-neuronal signalling in the mammalian brain. Nat. Commun. *5*.

Tekkök, S.B., Brown, A.M., Westenbroek, R., Pellerin, L., and Ransom, B.R. (2005). Transfer of glycogen-derived lactate from astrocytes to axons via specific monocarboxylate transporters supports mouse optic nerve activity. J. Neurosci. Res. *81*, 644–652.

Weber, B., and Barros, L.F. (2015). The Astrocyte: Powerhouse and Recycling Center. Cold Spring Harb. Perspect. Biol. a020396.

Wyss, M.T., Jolivet, R., Buck, A., Magistretti, P.J., and Weber, B. (2011). In Vivo Evidence for Lactate as a Neuronal Energy Source. J. Neurosci. *31*, 7477–7485.

Yang, J., Ruchti, E., Petit, J.-M., Jourdain, P., Grenningloh, G., Allaman, I., and Magistretti, P.J. (2014). Lactate promotes plasticity gene expression by potentiating NMDA signaling in neurons. Proc. Natl. Acad. Sci. *111*, 12228–12233.

Figure Legends

Figure 1. Expression of *Laconic* and *Pyronic in vivo*. (A top) 3D-Structure of the lactate sensor *Laconic*, which was excited with a pulsed laser (870 nm). Emission was collected for mTFP (450-475 nm) and for Venus (535-550 nm). (A bottom) The fluorescence (480 nm excitation, 505-565 nm emission, green) of four individual sensors was collected through a chronic cranial window preparation of the primary somatosensory cortex of a *C57BL/6* mice, scale bar: 1 mm. (B top) Serotype 6 adeno-associated viral vector (AAV6) with a *synapsin* promoter was used for neuronal expression, and serotype 9 vector (AAV9) with a *sGFAP* promoter for astrocytic expression. (B bottom) 2PLSM at 150 to 250 µm below the dura shows cell-type specific cytoplasmic sensor expression with nuclear exclusion (arrow heads), vascular end feet (arrows) and cellular processes (stars); scale bars: 50 µm. (C) The *in vitro* calibration curve of *Laconic* at 37°C shows substrate binding kinetics of lactate but no pH sensitivity. See also Figure S1A to E.

Figure 2. *Laconic* sensor functions *in vivo*. (A) *Laconic* signals increased both in astrocytes and neurons depending on the intravenously injected lactate dosage (Lac; 500 mM L-lactate solution; 0.5, 1 and 2 mmol per kg bodyweight; 0 mmol lactate was performed with 2 mmol per kg bodyweight of 500 mM sodium chloride solution). The standard deviations of cells in a single experiment (left) and of multiple independent experiments (right) are indicated (from 0 to 2 mmol/kg; normalization to individual baseline). See also Figure S1F, S1G, S3A and S3B. (B) Similarly, *Laconic* expressed in cultured astrocytes and neurons showed dose dependent signal increases. Data are normalized to pyruvate induced lactate depletion (see Figure S2D and S2E). Astrocytes but not neurons maintain sizable intracellular lactate levels even in a zero glucose and lactate medium, resulting in relatively low *Laconic* signal increases.

Figure 3. An intravenous injection of lactate increases *Laconic* signals more in neurons than in astrocytes. (A) Intravenous lactate infusions (4 mmol per kg bodyweight in 3 minutes, 500 mM solution) increased neuronal (5.7 ± 1.3%) more than astrocytic *Laconic* signal (4.3 ± 1.3%) in simultaneous recordings in one experiment (left) and over multiple recordings (right, normalization to individual baseline, mean on peak amplitudes, * = $p < 0.05$). See also Figure S3C. (B) The same lactate infusion protocol increased extracellular lactate (N = 6 animals, 0.27 ± 0.08 mM). (C) Blood lactate concentrations rose from 0.81 ± 0.26 mM to 17 ± 5.7 mM (N = 7 experiments). Data are represented as mean ± SD.

Figure 4. Baseline lactate levels in astrocytes and neurons can be compared by saturating *Laconic*. (A) Astrocytic and neuronal *Laconic* and *Pyronic* were simultaneously recorded during an intravenous infusion of ammonium chloride (4 mmol per kg bodyweight in 15 minutes, 500 mM solution) mixed with lactate (8 mmol per kg bodyweight in 15 minutes, 1 M solution), followed by a faster lactate injection (4 mmol per kg bodyweight in 3 minutes, 500 mM solution). *Pyronic* signals decreased during the ammonium chloride-lactate mix. In eight independent experiments, normalization to the saturation level of *Laconic* revealed lower baseline levels in neurons than in astrocytes (0.901 ± 0.024 vs. 0.931 ± 0.020, normalization to the three minutes after ammonium chloride stop, mean of baseline minima, * = $p < 0.05$). (B) Using the same infusion protocol, changes in extracellular lactate concentrations were measured in five trials. Extracellular lactate increased until the end of the infusion protocol by 0.87 ± 0.29 mM. Data are represented as mean ± SD. See also Figure S1H and S1I.

Figure 5. An intravenous injection of pyruvate decreases *Laconic* signals more in astrocytes than in neurons. (A) Intravenous pyruvate infusions (4 mmol per kg bodyweight in 3 minutes, 500 mM solution) decreased *Laconic* signal in astrocytes more than in neurons, while inducing only minor changes in *Pyronic* signal, as observed during simultaneous recordings in one experiment (left,

normalization to individual baseline). Similar effects were observed over multiple recordings (right, normalization to individual baseline, maximum decrease of astrocytes was 4.7 ± 1.5 and of neurons 0.6 ± 0.9 %, * = $p < 0.05$). (B) The same pyruvate infusion protocol increased extracellular lactate (N = 6 animals, 0.084 ± 0.02 mM). (C) The *Laconic* saturation protocol (see figure 4) was followed by a pyruvate infusion, which induced a decrease of astrocytic and neuronal *Laconic* signal and an increase in *Pyronic* signal. Normalization to three minutes after cessation of ammonium chloride infusion. (D) In some trials repetitive pyruvate infusions increased *Laconic* signal in neurons, possibly due to conversion of pyruvate to lactate. With this artificially increased neuronal lactate levels, a pyruvate infusion (2 mmol per kg bodyweight in 1 minute, 500 mM solution) induced trans-acceleration also in neurons. Normalization to last minute of trace. (E) Trans-acceleration occurs at monocarboxylate transporters (MCT), because the substrate binding site of MCTs switches at a higher rate to the other side of the membrane when a substrate is bound (MCT – S; k_2) than without a substrate bound (MCT; k_1). Therefore, any substrate of MCT on one side of the membrane increases the rate of transport of another substrate in the opposite direction. Data are represented as mean ± SD. See also Figure S2.

Figure 6. Model of lactate compartmentation. (A) Astrocytes accumulate lactate, which is transported along a concentration gradient via monocarboxylate transporters (MCT) to be consumed by neurons. Physiological (phys.) and experimentally increased (exp.) blood lactate levels are indicated. (B) Under artificially increased blood pyruvate levels, pyruvate enters brain cells from extracellular space via MCTs, forcing the extrusion of lactate. Pyruvate entry and concurrent lactate exit via MCTs requires relatively high intracellular lactate levels.

Figure 1

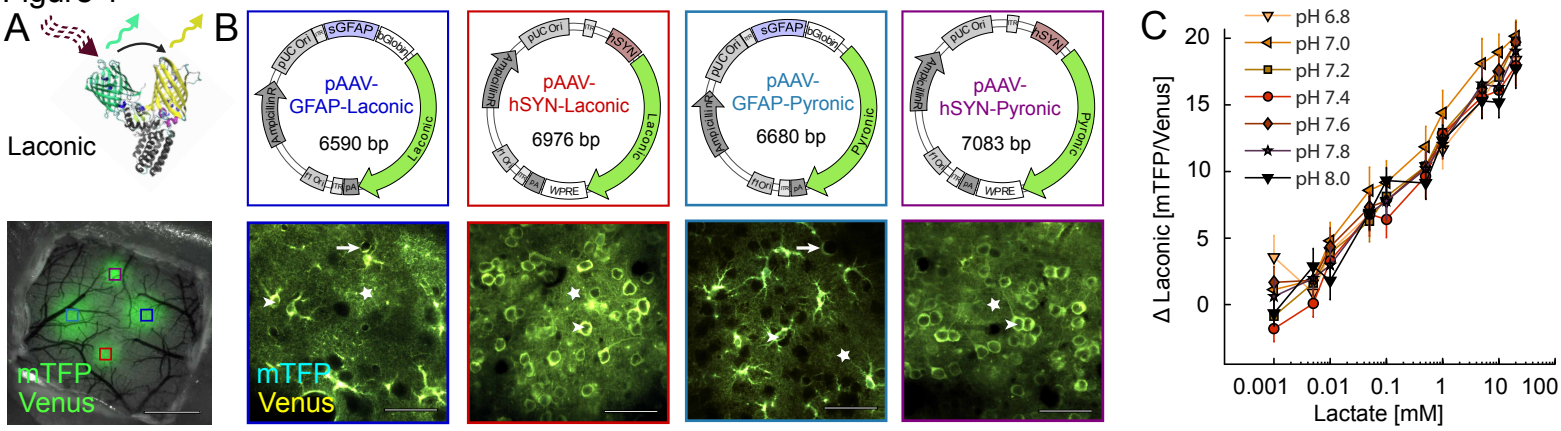
A
Laconic
mTFP
Venus
B
pAAV-
GFAP-Laconic
6590 bp
pAAV-
hSYN-Laconic
6976 bp
pAAV-
GFAP-Pyronic
6680 bp
pAAV-
hSYN-Pyronic
7083 bp
mTFP
Venus
C
pH 6.8
pH 7.0
pH 7.2
pH 7.4
pH 7.6
pH 7.8
pH 8.0
Δ Laconic [mTFP/Venus]
Lactate [mM]
0.001
0.01
0.1
1
10
100
0
5
10
15
20

Figure 2

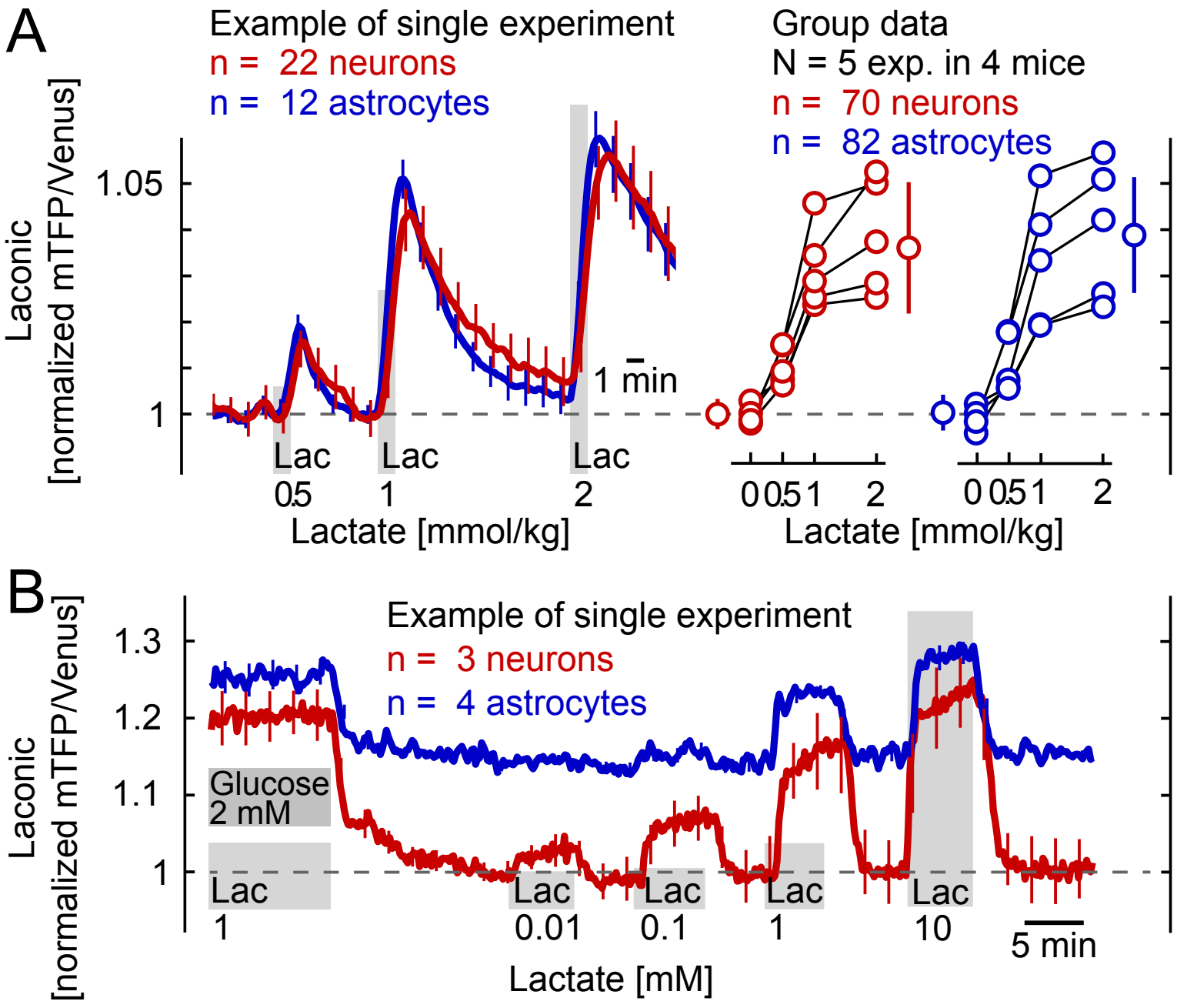
A
Example of single experiment
n = 22 neurons
n = 12 astrocytes
Group data
N = 5 exp. in 4 mice
n = 70 neurons
n = 82 astrocytes
Laconic
[normalized mTFP/Venus]
1.05
1
1 min
Lac
0.5
Lac
1
Lac
2
Lactate [mmol/kg]
0 0.5 1 2
0 0.5 1 2
Lactate [mmol/kg]
B
Example of single experiment
n = 3 neurons
n = 4 astrocytes
Laconic
[normalized mTFP/Venus]
1.3
1.2
1.1
1
Glucose
2 mM
Lac
1
Lac
0.01
Lac
0.1
Lac
1
Lac
10
5 min
Lactate [mM]

Figure 3

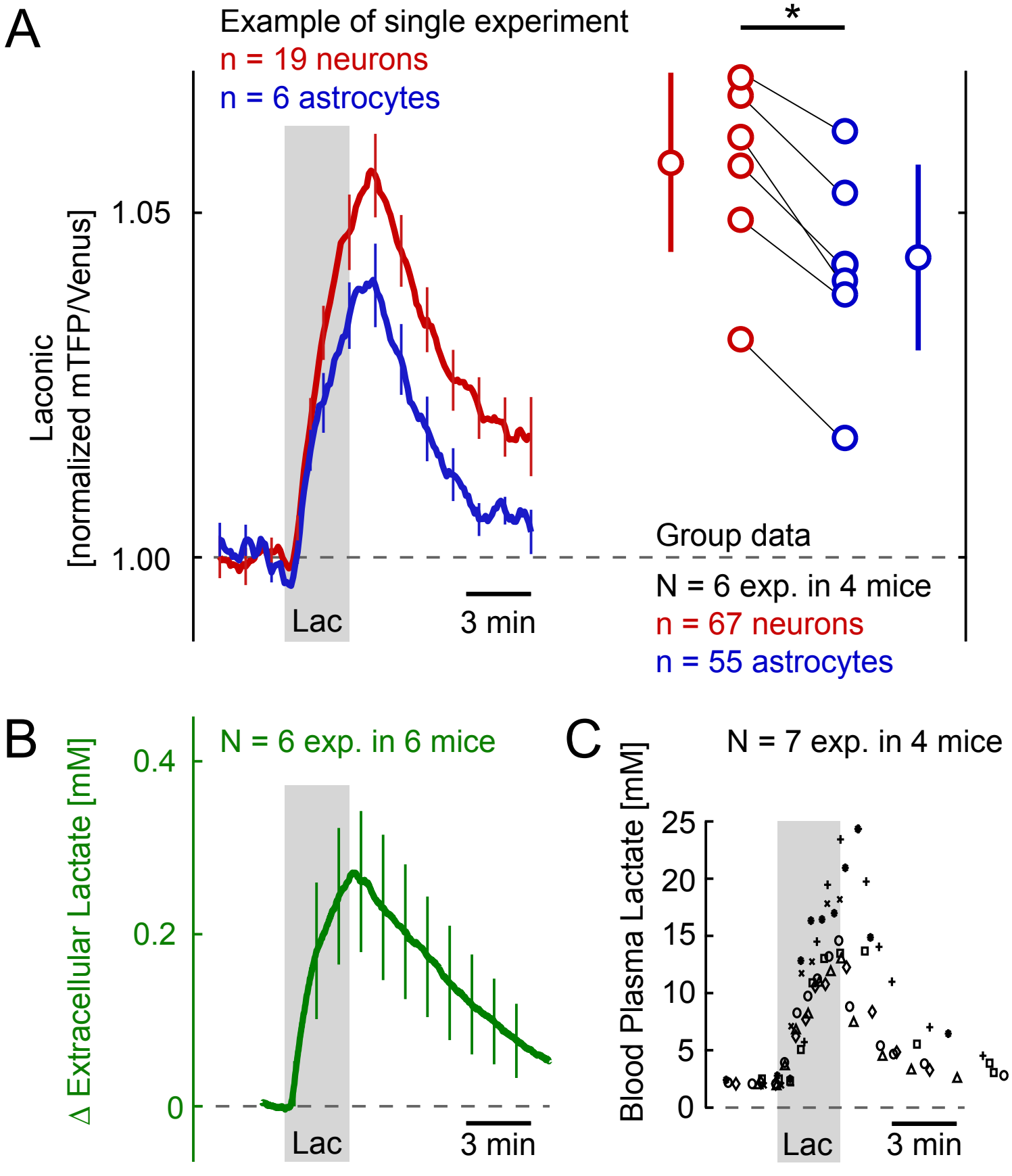
A
Example of single experiment
n = 19 neurons
n = 6 astrocytes
Laconic
[normalized mTFP/Venus]
1.05
1.00
Lac
3 min
*
Group data
N = 6 exp. in 4 mice
n = 67 neurons
n = 55 astrocytes
B
N = 6 exp. in 6 mice
Δ Extracellular Lactate [mM]
0.4
0.2
0
Lac
3 min
C
N = 7 exp. in 4 mice
Blood Plasma Lactate [mM]
25
20
15
10
5
0
Lac
3 min

Figure 4

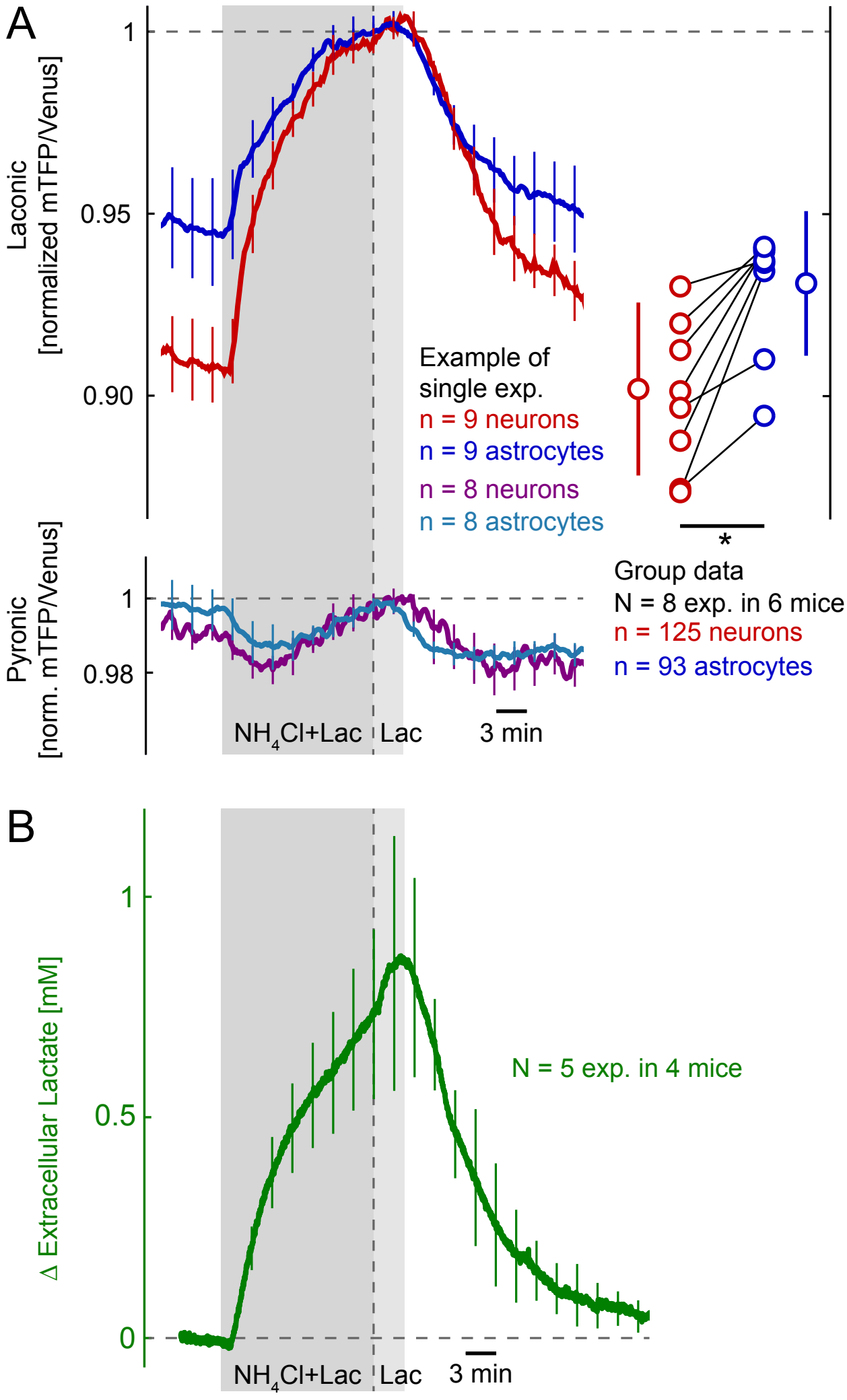
A
Laconic
[normalized mTFP/Venus]
1
0.95
0.90
Example of
single exp.
n = 9 neurons
n = 9 astrocytes
n = 8 neurons
n = 8 astrocytes
*
Group data
N = 8 exp. in 6 mice
n = 125 neurons
n = 93 astrocytes
Pyronic
[norm. mTFP/Venus]
1
0.98
NH4Cl+Lac
Lac
3 min
B
Δ Extracellular Lactate [mM]
1
0.5
0
N = 5 exp. in 4 mice
NH4Cl+Lac
Lac
3 min

Figure 5

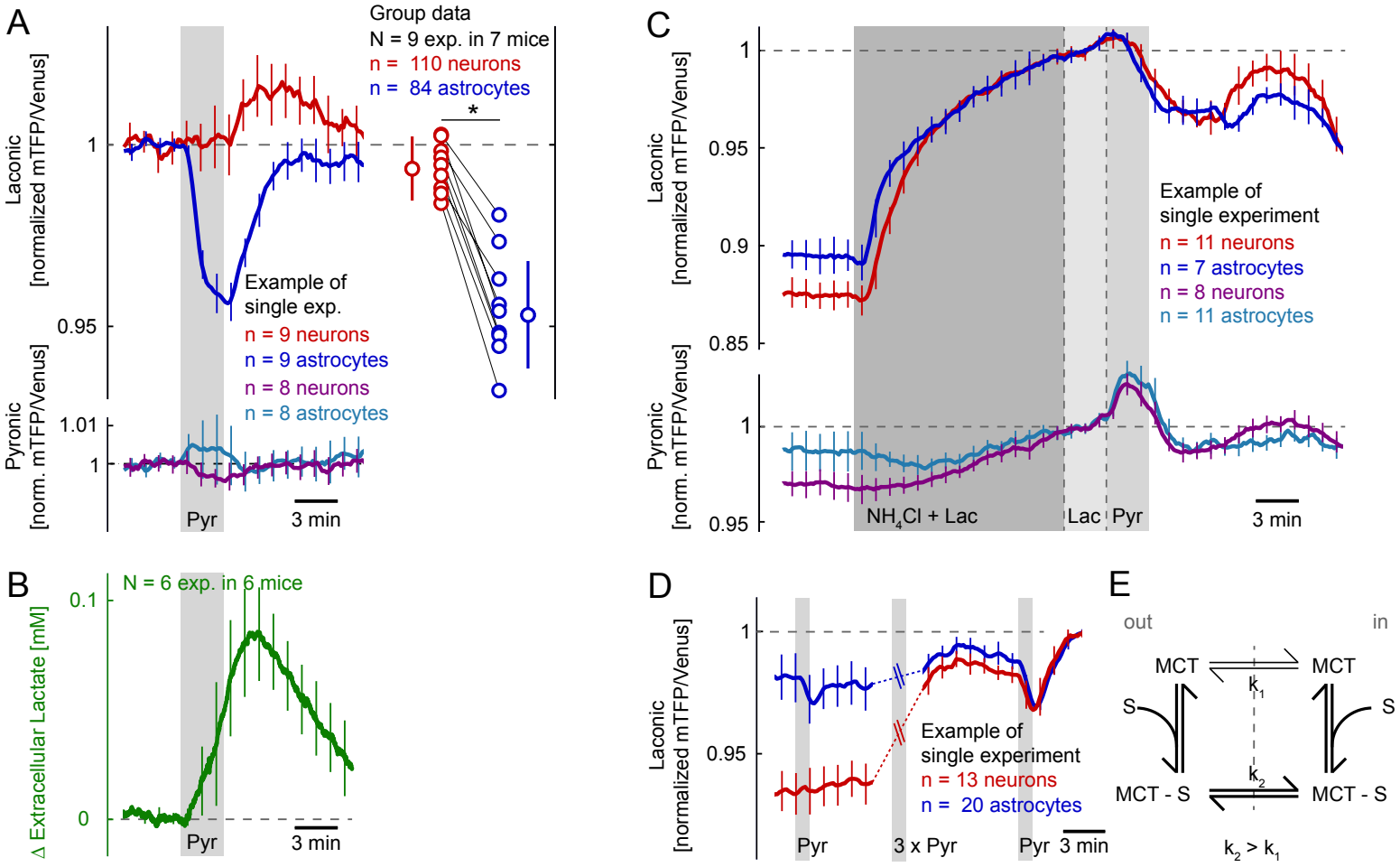
A
Group data
N = 9 exp. in 7 mice
n = 110 neurons
n = 84 astrocytes
*
Laconic
[normalized mTFP/Venus]
1
0.95
Example of
single exp.
n = 9 neurons
n = 9 astrocytes
n = 8 neurons
n = 8 astrocytes
Pyronic
[norm. mTFP/Venus]
1.01
1
Pyr
3 min
B
N = 6 exp. in 6 mice
0.1
0
Δ Extracellular Lactate [mM]
Pyr
3 min
C
Laconic
[normalized mTFP/Venus]
1
0.95
0.9
0.85
Example of
single experiment
n = 11 neurons
n = 7 astrocytes
n = 8 neurons
n = 11 astrocytes
Pyronic
[norm. mTFP/Venus]
1
0.95
NH4Cl + Lac
Lac
Pyr
3 min
D
Laconic
[normalized mTFP/Venus]
1
0.95
Example of
single experiment
n = 13 neurons
n = 20 astrocytes
Pyr
3 x Pyr
Pyr
3 min
E
out
in
MCT
MCT
S
S
k1
k2
MCT - S
MCT - S
k2 > k1

Figure 6

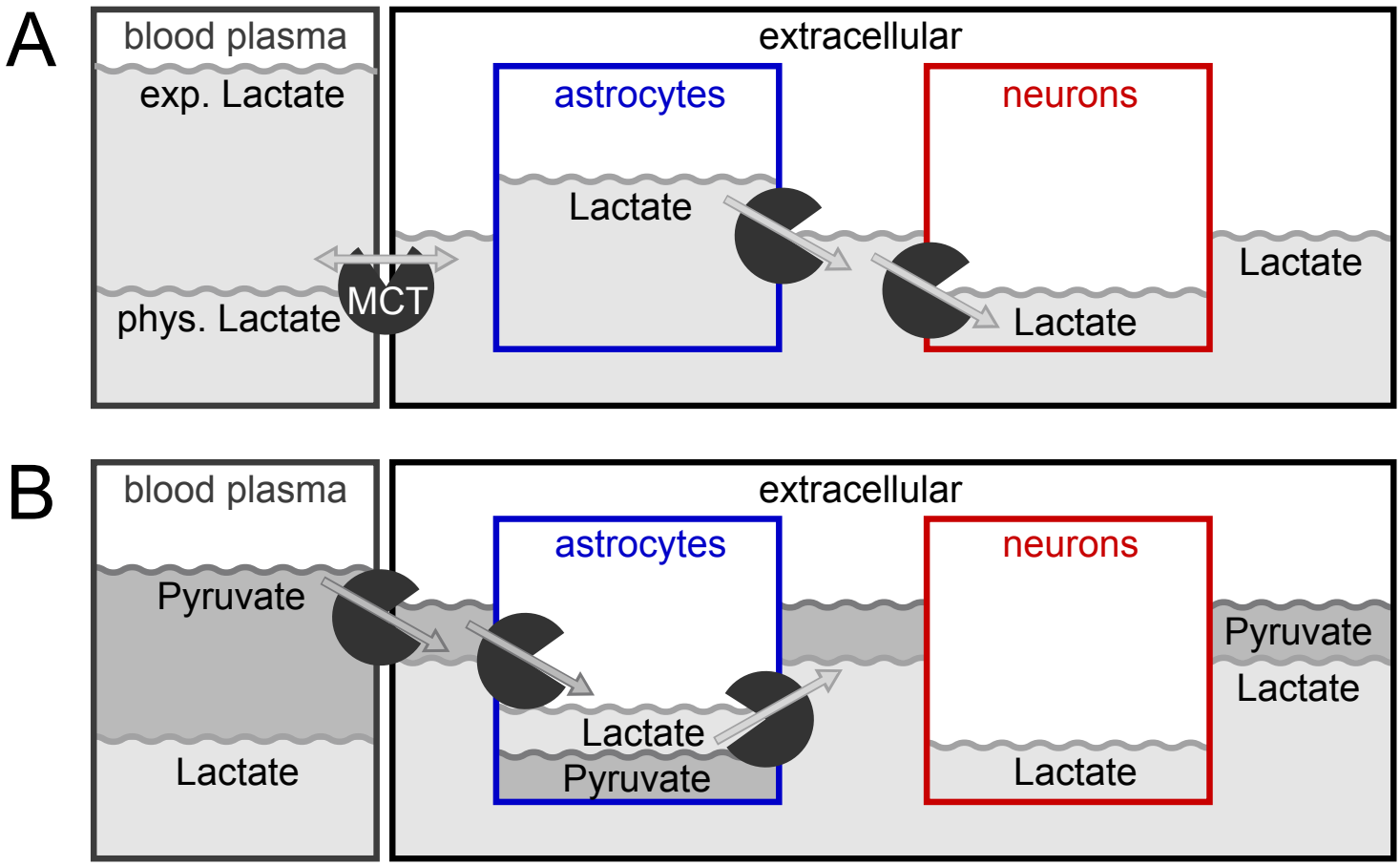
A
blood plasma
exp. Lactate
phys. Lactate
MCT
extracellular
astrocytes
Lactate
neurons
Lactate
Lactate
B
blood plasma
Pyruvate
Lactate
extracellular
astrocytes
Lactate
Pyruvate
neurons
Lactate
Pyruvate
Lactate

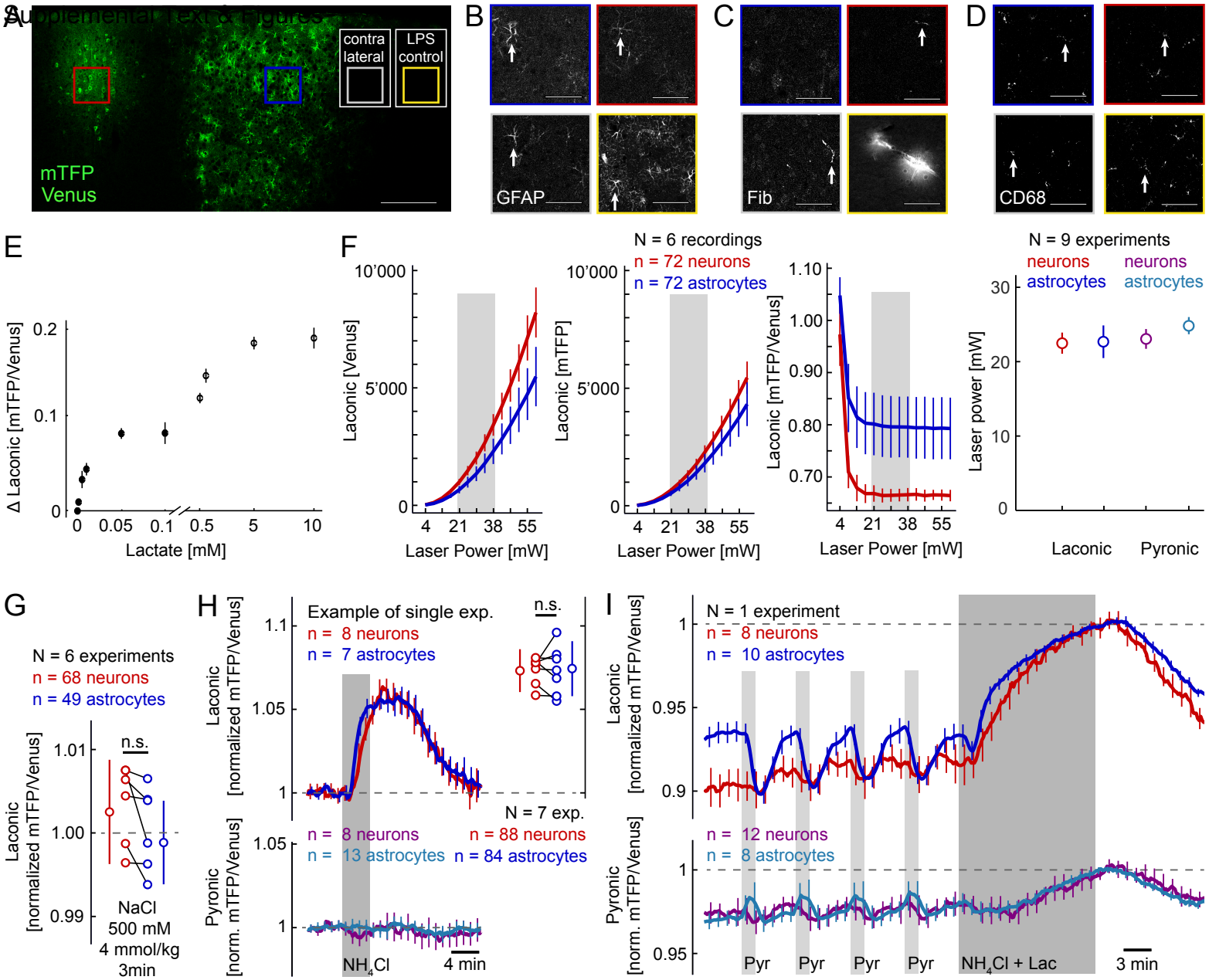
A
contra lateral
LPS control
mTFP
Venus
B
GFAP
C
Fib
D
CD68
E
Δ Laconic [mTFP/Venus]
Lactate [mM]
F
Laconic [Venus]
Laser Power [mW]
N = 6 recordings
n = 72 neurons
n = 72 astrocytes
Laconic [mTFP]
Laconic [mTFP/Venus]
N = 9 experiments
neurons
astrocytes
neurons
astrocytes
Laser power [mW]
Laconic
Pyronic
G
N = 6 experiments
n = 68 neurons
n = 49 astrocytes
Laconic [normalized mTFP/Venus]
n.s.
NaCl
500 mM
4 mmol/kg
3min
H
Example of single exp.
n = 8 neurons
n = 7 astrocytes
n.s.
N = 7 exp.
n = 8 neurons
n = 13 astrocytes
n = 88 neurons
n = 84 astrocytes
Laconic [normalized mTFP/Venus]
Pyronic [norm. mTFP/Venus]
NH4Cl
4 min
I
N = 1 experiment
n = 8 neurons
n = 10 astrocytes
n = 12 neurons
n = 8 astrocytes
Pyr
Pyr
Pyr
Pyr
NH4Cl + Lac
3 min

Figure S1. *Laconic* immunohistochemistry and specificity. Related to Figure 1, 3 and 4.

(A) Neuronal (left) and astrocytic (middle) *Laconic* fluorescence acquired *post mortem* using confocal microscopy. Cortical area without virus injection (right). Scale bar: 200 µm. (B) Both, astrocytic (blue frame) and neuronal (red frame) *Laconic* expressing tissue showed sparsely GFAP-positive astrocytes (arrows) without an increase compared to contralateral (gray frame) layer 2/3 cortex (image sections correspond to frame selections in panel A). The same GFAP staining was positive in mice injected with lipopolysaccharide (LPS, yellow frame), which is known to induce cortical inflammation (Fontana et al., 1981). (C) Fibrinogen staining was restricted to vessels (arrows) without any sign of blood brain barrier leakage as in LPS treated mice. (D) Staining for CD68 did not indicate an increased number or reactivity of microglia as with LPS treatment (arrows). Scale bars in figures B-D: 50 µm. (E) The *in vitro* calibration curve of *Laconic* shows the substrate binding kinetics of lactate at 25° celsius (San Martín et al., 2013). (F) Increasing the output laser power from 4 to 59 mW (measured under the objective) increased the fluorescence intensity in the *Venus* and *mTFP* channel, but did not affect ratio values at laser intensities used in this study (20 to 40 mW, grey bar). In the rightmost subpanel, laser power values measured in a set of experiments with pyruvate infusions are indicated. (G) The intravenous injection of sodium chloride (4 mmol per kg bodyweight in three minutes, 500 mM solution) did not show different signal changes in astrocytes and neurons (n.s. = $p > 0.05$). (H) Ammonium chloride (NH_4Cl) infusions over four minutes (2.5 mmol/kg bodyweight) increased *Laconic* signals in neurons and astrocytes (7.3 ± 1.3% vs. 7.4 ± 1.6%, respectively, normalization to baseline, mean of peak amplitudes, n.s. = $p > 0.05$). (I) Repetitive infusions of pyruvate (2 mmol per kg bodyweight in 1.5 minutes, 500 mM solution) were followed by the *Laconic* saturation protocol (ammonium chloride 4 mmol per kg bodyweight 500 mM solution mixed with lactate 8 mmol per kg bodyweight 1 M solution in 15 minutes). Normalization to the sensor's saturation point demonstrates the convergence of astrocytic and neuronal *Laconic* under pyruvate induced trans-acceleration (upper traces). The simultaneous measurement of the pyruvate sensor *Pyronic* demonstrates the specificity of *Laconic* to lactate (lower traces). Data are represented as mean ± SD.

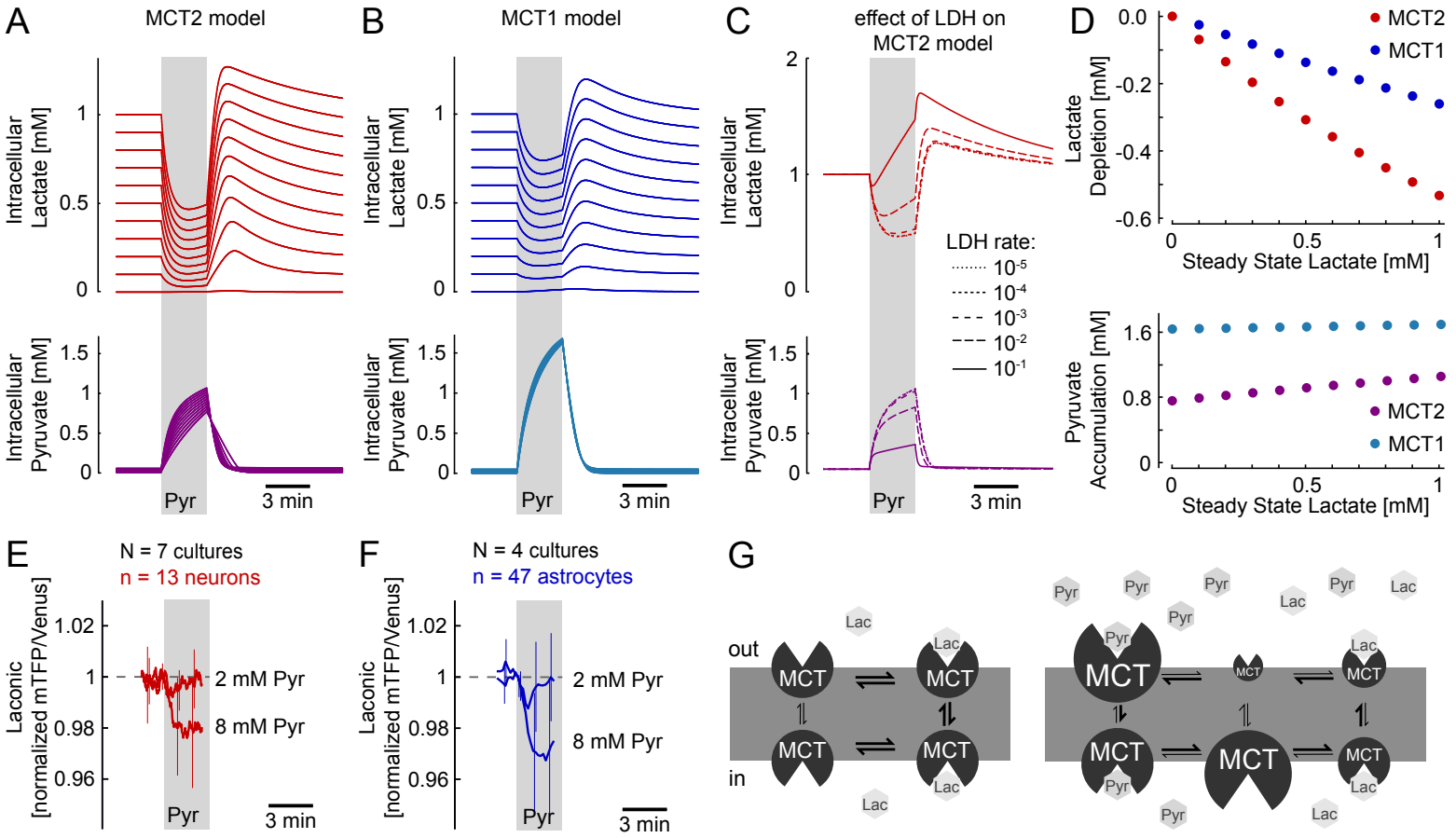
A
MCT2 model
Intracellular Lactate [mM]
Intracellular Pyruvate [mM]
Pyr
3 min
B
MCT1 model
C
effect of LDH on MCT2 model
LDH rate:
10-5
10-4
10-3
10-2
10-1
D
Lactate Depletion [mM]
MCT2
MCT1
Steady State Lactate [mM]
Pyruvate Accumulation [mM]
E
N = 7 cultures
n = 13 neurons
Laconic [normalized mTFP/Venus]
2 mM Pyr
8 mM Pyr
F
N = 4 cultures
n = 47 astrocytes
G
out
in
MCT
Lac
Pyr

Figure S2. In silico modeling of trans-acceleration and *in vitro* controls. Related to Figure 2 and 5.

Lactate and pyruvate are transported in and out of cells through monocarboxylate transporters (MCTs). Competition between the two substrates for the shared binding site in the transporter and the fact that the binding site trans-locates more efficiently when complexed with a substrate leads to trans-acceleration (also known as accelerated exchange (Garcia et al., 1994), that is the enhancement of transport of a substrate located at the opposite side of the membrane. Trans-acceleration can be explained with the following kinetic model: (A) Simulation results of intracellular lactate and pyruvate concentrations using kinetic parameters of the MCT 2 (4 µM; symmetrically distributed; pH 7.4; K_{off} lactate 7.6 x 10^6 s^{-1} and K_{off} pyruvate 7.6 x 10^5 s^{-1}) during an extracellular 2 mM pyruvate challenge. Each line represents a different steady state lactate concentration from 0 to 1 mM at baseline. The rate of LDH is set to 10^{-4} s^{-1} and the reverse reaction 20 times lower, putting the ratio lactate/pyruvate to 20. (B) The same model as before but with the kinetic parameters of MCT 1 (20 µM; symmetrically distributed; pH 7.4; K_{off} lactate 7.6 x 10^7 s^{-1} and K_{off} pyruvate 7.6 x 10^6 s^{-1}). (C) The contribution of LDH activity on pyruvate induced transients in the MCT 2 model is demonstrated for a wide range of LDH rates. (D) In the two MCT models, the amplitude of lactate depletion after 20 s depends linearly on the baseline lactate level and is larger with MCT 2 than MCT 1 (top). Pyruvate accumulates more in the MCT1 model (bottom). (E) Cultured neurons expressing *Laconic* showed pyruvate dose dependent lactate depletion (cells in a Krebs Ringer Hepes Bicarbonate buffer with 2 mM glucose and 1 mM lactate). (F) Cultured astrocytes in the same buffer solution showed similar *Laconic* transients. Data are represented as mean ± SD. (G) Under physiological conditions pyruvate concentrations are too low to compete with lactate at MCTs (left). After a rise in extracellular pyruvate (right part), the transporters bind pyruvate, which results in a reduced binding site availability for lactate and a reduction of lactate influx. Then the binding site trans-locates from outward-facing to inward-facing configuration. If there is lactate within the cell, the increased number of inward-facing sites subsequently causes an increased lactate efflux. The combination of reduced lactate influx and increased lactate efflux results in a drop of intracellular lactate concentration. This increase of lactate flux by pyruvate in this example is analogous to the extrusion of calcium by sodium in the Na^+-Ca^{2+} exchanger.

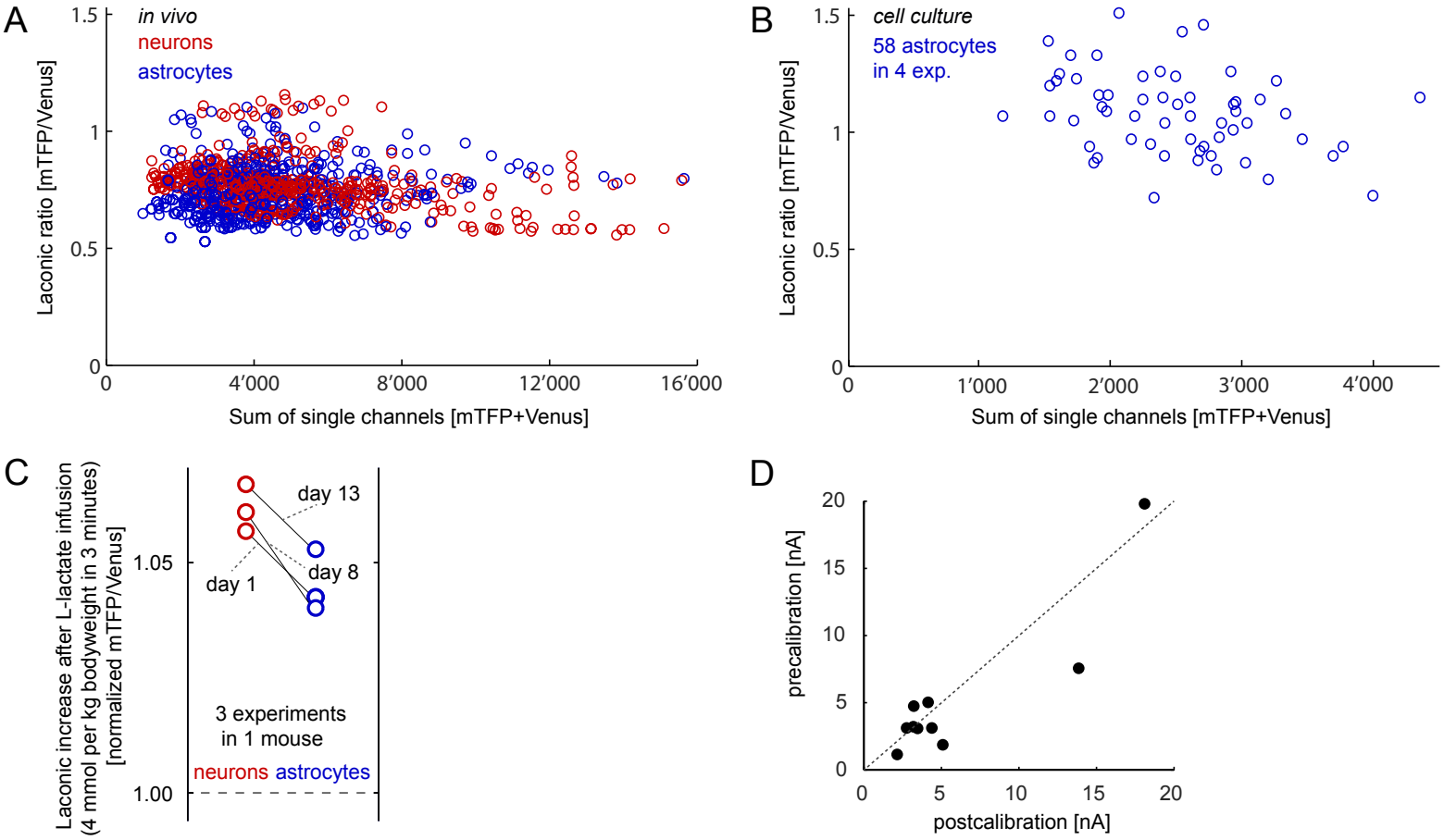
A
in vivo
neurons
astrocytes
Laconic ratio [mTFP/Venus]
Sum of single channels [mTFP+Venus]
0
0.5
1
1.5
4'000
8'000
12'000
16'000
B
cell culture
58 astrocytes
in 4 exp.
Laconic ratio [mTFP/Venus]
Sum of single channels [mTFP+Venus]
1'000
2'000
3'000
4'000
C
Laconic increase after L-lactate infusion
(4 mmol per kg bodyweight in 3 minutes)
[normalized mTFP/Venus]
1.05
1.00
day 13
day 8
day 1
3 experiments
in 1 mouse
neurons astrocytes
D
precalibration [nA]
postcalibration [nA]
0
5
10
15
20

Figure S3. Characterization of intracellular and extracellular lactate measurements. Related to Figure 2, 3, 4 and 5.

(A) and (B) demonstrate that the Laconic FRET ratio is independent from sensor expression levels. (A) A sample measurement from baseline (frame 10) from each cell imaged in this study was taken and the sum of the two channels was plotted against their ratio. (B) The same plot is given for cultured astrocytes. (C) Demonstration of reproducibility over different imaging sessions. Repetitive lactate infusions in a single mouse on day 1, 8 and 13 increased *Laconic* signals in variable populations of layer 2/3 neocortical neurons and astrocytes. (D) Comparison of the *in vitro* pre- and post- calibration values from the extracellular lactate biosensors used *in vivo* demonstrates that the sensitivity of the sensor was preserved within an experiment.

Supplemental References

Fontana, A., Bosshard, R., Dahinden, C., Grob, P., and Grieder, A. (1981). Glia cell response to bacterial lipopolysaccharide: Effect on nucleotide synthesis, its genetic control and definition of the active principle. J. Neuroimmunol. *1*, 343–352.

Garcia, C.K., Goldstein, J.L., Pathak, R.K., Anderson, R.G.W., and Brown, M.S. (1994). Molecular characterization of a membrane transporter for lactate, pyruvate, and other monocarboxylates: Implications for the Cori cycle. Cell *76*, 865–873.

San Martín, A., Ceballo, S., Ruminot, I., Lerchundi, R., Frommer, W.B., and Barros, L.F. (2013). A Genetically Encoded FRET Lactate Sensor and Its Use To Detect the Warburg Effect in Single Cancer Cells. PLoS ONE *8*, e57712.